



Assimilation of sea surface salinities from SMOS in an Arctic coupled ocean and sea ice reanalysis

Jiping Xie¹, Roshin P. Raj¹, Laurent Bertino¹, Justino Martínez², Carolina Gabarró^{2,3}, and Rafael Catany⁴

¹ Nansen Environmental and Remote Sensing Center and Bjerknes Centre for Climate Research, Bergen, Norway

² Institute of Marine Sciences, ICM-CSIC, Barcelona, Spain

³ Barcelona Expert Center, Barcelona, Spain

⁴ ARGANS, Plymouth, UK

Corresponding author: Jiping Xie, jiping.xie@nersc.no



1

Abstract

2 In the Arctic, the sea surface salinity (SSS) plays a key role in processes related to
3 water mixing and sea ice. However, the lack of salinity observations causes large
4 uncertainties in Arctic Ocean forecasts and reanalysis. Recently the Soil Moisture and Ocean
5 Salinity (SMOS) satellite mission was used by the Barcelona Expert Centre to propose an
6 Arctic SSS product.

7 In this study, we evaluate the impact of assimilating this data in a coupled ocean-ice data
8 assimilation system. Using the Ensemble Kalman filter from July to December 2016, two
9 assimilation runs assimilated two successive versions of the SMOS SSS product, on top of a
10 pre-existing reanalysis run. The runs were validated against independent in situ salinity
11 profiles in the Arctic. The results show that the biases and the Root Mean Squared
12 Differences (RMSD) of SSS are reduced by 10% to 50% depending on areas and put the
13 latest product to its advantage. The time series of Freshwater Content (FWC) further show
14 that its seasonal cycle can be adjusted by assimilation of the SSS products, which is
15 encouraging for its use in a long-time reanalysis to monitor the Arctic water cycle.

16

17 **Keywords:** Arctic Ocean; Sea Surface Salinity; FWC; SMOS;



18 **1. Introduction**

19 The Arctic Ocean is undergoing a dramatic warming, causing the loss of sea ice area
20 coverage visible on satellite data (Johannessen et al., 1999; Stroeve and Notz, 2018). The
21 sea ice melt contributes freshwater to the Arctic Ocean, together with other sources and has
22 far-reaching effects on the Arctic Ocean environment, as reviewed in Carmack et al. (2016).
23 A recent update of the review paper showed a stabilization of the Freshwater Content (FWC)
24 of the Arctic Basin, although observations indicate that the Beaufort Gyre keeps freshening
25 (Solomon et al., 2021). The Arctic observing system, contrary to other oceans, lacks the
26 capability to provide a complete picture of the ocean salinity, particularly because of
27 obstruction by sea ice.

28 A complete reconstruction of Arctic environmental variables requires a data assimilative
29 numerical model capable of propagating information below sea ice during the winter as
30 practiced by ocean operational forecast systems (Dombrowsky, 2009; Fujii et al., 2019). As
31 for other ocean data assimilation (DA) applications, the Arctic reanalysis products of ocean
32 and sea ice play an important role in understanding climate change and its mechanisms. In
33 recent years, many studies (Storto et al., 2019; Uotila et al., 2019) evaluated the quality of
34 the Arctic reanalysis products and recommended experiments maximizing the usefulness of
35 new available observations, such as done in Kaminski et al. (2015) or Xie et al. (2018)
36 among others. However, there are no impact studies of salinity observations in the Arctic to
37 our knowledge.

38 Ocean salinity has been used to study the water cycle for the last 20 years (e.g., Curry et al.,
39 2003; Boyer et al., 2005; Yu, 2011; Yu et al., 2017). The salinity variations have far-reaching
40 implications for ocean mixing, water mass formation, and ocean general circulation, but still
41 suffer from large uncertainties, mainly due to sparse observations and the lack of a steady-
42 state reference time period (e.g., Stroh et al., 2015; Xie et al., 2019). Measuring sea surface
43 salinity (SSS) from passive microwave remote sensing is a comparatively new but promising
44 way to reduce the uncertainty in salinity. Launched in November 2009, the Microwave
45 Imaging Radiometer using Aperture Synthesis (MIRAS) instrument of the European Space
46 Agency's (ESA) Soil Moisture and Ocean Salinity (SMOS) mission measures the brightness
47 temperature (T_B) on the sea surface. The passive 2-D interferometric radiometer on the
48 satellite operating in L-band (1.4 GHz) is sensitive to water salinity and sufficiently free from
49 electromagnetic interference (e.g., Font et al., 2010; Kerr et al., 2010). Since May 2010,
50 SMOS operationally provides SSS records over the global ocean (Mecklenburg et al., 2012).
51 Furthermore, the assimilation of satellite derived SSS products using an ensemble DA
52 method has been found to significantly improve the surface and subsurface salinity fields in
53 the tropics (Lu et al. 2016). The advantages of assimilating three SSS products from SMOS,
54 Aquarius (ref., Lee et al, 2012), and Soil Moisture Active Passive Mission (SMAP; e.g., Tang



55 et al., 2017) into a global ocean forecast system using 3D-Var DA method have also been
56 demonstrated by Martin et al (2019). Their results show benefits of assimilating both the
57 SMOS and SMAP datasets in the intertropical convergence zone in the tropical Pacific.
58 However, there are very few studies to investigate the impacts of assimilating SSS products
59 in Arctic or high latitudes. There are three main reasons for this: i) the lower sensitivity of T_B
60 in cold waters leading to larger SSS error (Yueh et al., 2001) (e.g, the sensitivity drops from
61 0.5 to 0.3 K PSU⁻¹ when the sea surface temperature decreases from 15 to 5°C); ii) Land-
62 sea and ice-sea contaminations resulting from the abrupt changes of T_B values across
63 these two interfaces, combined with the large ground footprint of SMOS; and iii) The removal
64 of biases ideally requires a well-observed steady-state period, from which climate change
65 has deprived us. Addressing these challenges in the SMOS salinity retrieval approach,
66 Olmedo et al. (2017) introduced a non-Bayesian retrieval method to debias the Level 1
67 baseline (L1B) salinity against the reference SSS from Argo data.
68 Starting from ESA L1B (v620) product of T_B from SMOS, the Barcelona Expert Centre (BEC)
69 released the version 2 Arctic gridded SSS product with a regular grid by 25 km resolution
70 (e.g., Olmedo et al., 2018) via their portal (<http://bec.icm.csic.es/>; last accessed March 2019).
71 The V2 SSS regional product was produced for the Arctic domain during the time-period
72 2011-2016. Xie et al. (2019) evaluated this earlier SSS product and found considerable
73 discrepancies among the six SSS products in the Arctic, especially in the freshest seawater
74 (<24 psu). The intercomparison of these Arctic SSS products shows room for improvement
75 of the SMOS-based SSS in the Arctic.
76 Recently, under the framework of the ESA project Arctic+Salinity and further developing the
77 non-Bayesian scheme, the effective resolutions were enhanced both in space and time. The
78 new version of SSS product (V3.1) shows advantages for monitoring the mesoscale
79 structures and the river discharges (e.g., Martínez et al., 2022), and was released through
80 the BEC portal (also at doi: [10.20350/digitalCSIC/12620](https://doi.org/10.20350/digitalCSIC/12620); last accessed May 2022). It also
81 provides daily maps of 9-days averages in the Arctic on the regular 25 km grid and covers a
82 longer time-period 2011-2019. The major differences in the estimation of the two SSS
83 products (V2.0 and V3.1) are detailed in the Algorithm Theoretical Baseline Document
84 (ATBD) of the Arctic+Salinity project (Martínez et al., 2020). Another SMOS-based Arctic
85 surface salinity product from LOCEAN (Supply et al. 2020, Boutin et al., 2022) has been
86 released posterior to Xie et al. (2019), but not assimilated in this study.
87 The two successive versions of the BEC SMOS SSS products are assimilated in the
88 TOPAZ4 Arctic reanalysis system during the summer 2016, and compared to the Arctic
89 reanalysis without assimilation of satellite SSS data, which consists the Arctic reanalysis in
90 the Copernicus Marine Services at that time. The model validation against independent



91 observations will show the differences stemming from these two products, although they are
92 originating from the same initial data source (SMOS). Their effect once assimilated in an
93 Arctic coupled ice-ocean model shows large differences, thereby also motivating further
94 efforts to improve SSS retrievals in the cold Arctic.
95 The paper is organized as follows: Section 2 describes briefly the coupled ocean and sea ice
96 data assimilation system and the assimilation experiments; Section 3 describes the in situ
97 observations and the validation metrics; The results are presented in Section 4 which
98 includes the validation using independent SSS observations, separated into different ocean
99 basins. Section 4 also analyses the impact of the assimilation using the regional SSS
100 assimilation increments, and explores the integrated effect on the freshwater contents in the
101 model. In Section 5, the findings of this study and future perspectives are summarized.

102

103 **2. Assimilation system and experimental design**

104 *2.1 The Arctic ocean and sea-ice coupled data assimilation system*

105 TOPAZ was built as a coupled ocean and sea ice data assimilation system, using the
106 ensemble Kalman filter method (EnKF; Evensen 2003) to assimilate consistently multiple
107 types of observations in the ocean and sea ice (Xie et al., 2017). The ocean model in this
108 system uses the version 2.2 of the Hybrid Coordinate Ocean Model (HYCOM; Chassignet et
109 al., 2003) with a low-distortion square grid of horizontal resolution of 12-16 km. The coupled
110 sea ice model uses a single category thermodynamic model (Drange and Simonsen, 1996)
111 combined with the dynamics of the modified elastic-viscous-plastic rheology (Bouillon et al.,
112 2013). The model covers the whole Arctic basin excluding the Pacific Ocean. A seasonal
113 inflow is imposed across Bering Strait, based on observed transports (Woodgate et al.,
114 2012). At all lateral boundaries, the temperature and salinity stratifications are relaxed to a
115 climatology combining the 2013 World Ocean Atlas (version 2.0 of WOA13; Zweng et al.,
116 2013) and the Polar science center Hydrographic Climatology version 3.0 (PHC; Steele et al.,
117 2001) with a 20-grid cells buffer zone. To avoid a potential model drift, the surface salinity is
118 relaxed to the same climatology with a 30-day timescale, and the relaxation is turned off
119 wherever the difference from climatology exceeds 0.5 psu. The salinity flux from the SSS
120 relaxation thus spreads evenly into the mixed layer depth without creating a new stable fresh
121 layer at the surface.

122 The TOPAZ model runs an ensemble of 100 members. On a weekly basis, the
123 Deterministic Ensemble Kalman Filter (DEnKF; Sakov et al., 2012) then assimilates different
124 types of ocean and ice observations, including along-track sea level anomaly (SLA), sea
125 surface temperature (SST), in situ profiles of temperature and salinity, sea ice concentrations
126 (SIC) and sea ice drift products all sourced from the Copernicus Marine Environment



127 Monitoring Services (CMEMS). The two steps of the assimilation system can be simply
128 translated by the following expressions (update and model propagation):

$$129 \quad X_a = X_f + K(y - HX_f) \quad (1)$$

$$130 \quad X_f = M(X_a) \quad (2)$$

131 Where the matrix \mathbf{X} represents the model states with all 3-D and 2-D variables needed by
132 the model forward integration, represented by the operator \mathbf{M} . The subscripts 'a' and 'f'
133 respectively indicate the analyzed model state obtained through optimization after DA, and
134 the model forecast. The vector y is composed of the quality-checked observations during the
135 weekly cycle, the observation operator H gives the model equivalent matching the
136 observations. The innovation term (in parenthesis in Eq.1) represents the differences
137 between the model and the various observations on the observation space. The \mathbf{K} matrix
138 (Kalman gain), is calculated as in Sakov et al. (2012) and updated in Xie et al. (2017). The
139 same TOPAZ4 system provides a 10-days' forecast of ocean physics and biogeochemistry in
140 the Arctic everyday via the CMEMS portal.

141

142 *2.2 The assimilation experiments and the observation error estimate for SSS*

143 To evaluate the impact of the two versions of the SSS products, a control assimilation
144 experiment (Exp0) and two parallel assimilation experiments (ExpV2, ExpV3) were
145 performed in the time period from July to December 2016. Exp0 assimilates all available
146 ocean and sea ice data, except the satellite SSS product. On the other hand, ExpV2 and
147 ExpV3 additionally assimilate the BEC SSS product V2.0 and V3.1 respectively. The main
148 differences of the three assimilation runs of ExpV2 and ExpV3 are detailed in Table 1.
149 Since the salinity errors from Passive Microwaves are higher in high latitudes than
150 elsewhere, the zonal average of standard errors north of 60°N were previously estimated
151 around 0.6 psu (Vinogradova et al., 2014). Later on, the intercomparison of different SSS
152 products including the climatology, satellite, and the Exp0 reanalysis showed that the
153 discrepancies were a decreasing function of salinity (Xie et al., 2019). This relationship
154 seems qualitatively reasonable as the spatio-temporal variability and representativity errors
155 are often higher in areas of fresher water, but quantitatively they combine the errors of the
156 remote sensing products, models and climatologies and may be larger than the remote
157 sensing errors alone. Still, we use an error function for ExpV2 and ExpV3 adjusted to the
158 discrepancies as shown in Eq. 3:

$$159 \quad \delta_{SSS} = \max \left\{ \delta_{int}, \left[0.6 + \frac{6}{1 + \exp\left(\frac{SSS-16}{5}\right)} \right]^2 \right\} \quad (3)$$

160 Where δ_{int} is the instrumental error variance estimated by the data provider. In ExpV2, it is
161 set to zero due to their absence. Eq. 3 yields more conservative error estimates than the
162 providers, which also reduce the inconsistencies caused by strong assimilation updates.



163 Other such precautions are applied following Sakov et al. (2012). By construction, the
164 observation errors are always larger for the V3.1 than the V2 product, but in fresh waters
165 they are identical. This implies that the assimilation may pull the analysis closer to the V2
166 than the V3.1 product in the more saline waters but are otherwise treated on equal footing,
167 ignoring that the more recent product is a priori expected to be more reliable.

168

169 **3. In situ SSS observations for validation**

170 All in situ salinity profiles were collected from various repositories and cruises (as shown in
171 Fig. 1). The salinity measurements were extracted near the surface over the Arctic domain
172 during the experimental time period and sanity-checked. Since the model does not reproduce
173 local gradients of the vertical salinity profiles shown in Supply et al. (2020), all the salinity
174 profiles are averaged over the upper 8 meters below the surface. This also avoids the loss of
175 the profiles that do not reach the surface.

- 176 • *Data from the Beaufort Gyre Experiment Project (BGEP)*

177 The BGEP has maintained an observing system in the Canadian Basin since 2003 and
178 provides in-situ observations over the Beaufort Gyre every summer. Although the BGEP has
179 maintained three bottom-tethered moorings since 2003, the shallowest depth of the
180 measured profiles for temperature and salinity is below 50 m. Hence, in this study, we only
181 use the Conductivity Temperature Depth (CTD) dataset from the cruise in 2016
182 (<https://www2.who.edu/site/beaufortgyre/data/ctd-and-geochemistry/>, last access: 14th
183 February 2022). SSS observations from these CTD profiles in the time-period from 13th Sep
184 to 10th Oct 2016 are represented by the red triangles in Fig.1.

- 185 • *Data from Oceans Melting Greenland (OMG)*

186 The project Oceans Melting Greenland was funded by NASA to understand the role of the
187 ocean in melting Greenland's glaciers. Over a five-year campaign, this project collected
188 temperature and salinity profiles by Airborne eXpendable Conductivity Temperature Depth
189 (AXCTD) launched from an aircraft (e.g., Fenty, et al, 2016). The deployed probe can sink to
190 a depth of 1000 meters, connected with a float by a wire. The measured temperature and
191 conductivity are then sent back to the aircraft. These salinity profiles collected during the first
192 OMG campaign in 2016, are downloaded from
193 https://podaac.jpl.nasa.gov/dataset/OMG_L2_AXCTD/ (last access: 10th February 2022). The
194 SSS from OMG distributed around Greenland, from 13th Sep to 10th Oct 2016 are shown as
195 the inverted red-triangles in Fig. 1.

- 196 • *Data from the International Council for the Exploration of the Sea (ICES)*

197 Salinity profiles were also obtained from the ICES portal (<https://www.ices.dk>). Shown as
198 blue squares in Fig. 1, the locations of the profiles during the last 6 months of 2016 are



199 dense in the Nordic Seas, and restricted to the north of 58°N for this study. Valid salinity
200 profiles from ICES (last access: 9th February 2022), are obtained from 6th July to 23rd Nov in
201 2016.

202 • *Data from other cruises at the Arctic Data Center (ADC)*

203 Surface salinity observations from scientific cruises are obtained from the Arctic Data
204 Center portal (<https://arcticdata.io/catalog/data>; last access: 17th Feb 2022). During the
205 model experiment, the first relevant cruise in ADC was SKQ201612S which was operated by
206 University of Alaska Fairbanks with the RV Sikuliaq. This cruise collected data from Nome,
207 Alaska on 3rd September, to the northeast Chukchi Sea, and then back to Nome at the end of
208 September 2016. The temperature and salinity profiles were collected by a Sea-Bird 911
209 CTD instrument package. All measurements at each station were done both down- and up-
210 cast ways. To produce water column profiles at each station, the down-cast data were
211 binned at 1 m intervals (Goñi et al., 2021). Besides the CTD profiles of SKQ201612S, more
212 seawater samples were collected via the surface underway system on the RV Sikuliaq.
213 Through a sea chest below the waterline (eg., 4-8 m), the uncontaminated seawater was
214 pumped into the ship and the corresponding filtration system supplies samples every 3 hours
215 to the sensors (More details in Goñi et al., 2019). These SSS observations were obtained
216 from 9th to 27th September, indicated as blue crosses in Fig. 1.

217 Moreover, SSS measurements were also collected from the Seabird CTD on board Sir
218 Wilfrid Laurier (SWL) vessel but only in July 2016. This cruise is part of the annual monitoring
219 from the Canadian Coast Guard Service (Cooper et al., 2019). The SSS observations are
220 obtained near the Bering Strait close to the Pacific boundary of our model.

221 After removing the effect of diurnal cycle in observed surface salinity, all valid SSS
222 measurements from the above data sources are compared with the daily average SSS of the
223 three assimilation experiments listed in Table 1. All the assimilation runs use a weekly
224 assimilation cycle: the model runs forward 7 days after each assimilation step and provides
225 daily averages for each day from the ensemble mean, which we refer to as “forecast” even
226 when using delayed-mode observations and atmospheric forcings. The model data has been
227 collocated with the observations for validation. To estimate the forecast differences to
228 observations, we use the standard statistical moments:

229
$$Bias = \frac{1}{N} \sum_{i=1}^N (H\bar{X}_i - y_i) \quad (4),$$

230
$$RMSE = \frac{1}{N} \sum_{i=1}^N (H\bar{X}_i - y_i)^2 \quad (5),$$

231 Where i is the i th day, N represents the total number of days depending on the

232 observations, and \mathbf{X}_i represents the model daily average at the time of the observation y_i .

233 The \mathbf{X}_i bar denotes the ensemble mean using 100 model members here, and the operator H



234 extracts the model SSS at the observed location. The model performance can then be
235 quantitatively compared among the three assimilation runs.

236

237 **4. Results**

238 *4.1 Diagnosing using assimilation statistics*

239 *The SSS innovations* in the two assimilation runs, ExpV2 and ExpV3, are shown in Fig. 2,
240 together with the number of assimilated SSS observations and the ensemble spread of SSS
241 calculated by the ensemble standard deviation. The total number of observations is
242 maximum in September when the sea ice cover is minimal. Since both versions of the SSS
243 product share the same time frequency (9 days average) and gridded format, the number of
244 assimilated observations in the two runs are identical (gray lines in Fig. 2). For ExpV2, the
245 Root Mean Square (RMS) of the innovation varies between 0.4 and 1.2 psu, but the mean of
246 innovation which is the opposite of the bias (Eq. 1) shows a positive salinity bias, especially
247 during September, when the saline bias is around 0.4 psu. However in ExpV3 the salinity
248 bias quickly disappears after a few data assimilation cycles. The RMS of the innovation are
249 larger in ExpV3 between 0.6 and 1.6 psu, which can partly be explained by the higher
250 effective resolution of the V3.1 product. In ExpV3, the RMS of the SSS innovation (the red
251 line) jumps down after the first SSS assimilation step. The RMS of innovations and the
252 observation errors both decrease from summer to winter, following a yearly cycle as the
253 areas of fresher water get gradually ice-covered. The domain-averaged observation errors
254 are only slightly larger in ExpV3 than in ExpV2, as explained above, and the RMS of
255 innovations become lower than the observation errors near the end of the run, which
256 indicates that the observations errors sound overestimated.

257 Figure 3 shows SSS maps from the two SSS assimilation runs (ExpV2 and ExpV3) and the
258 control run (Exp0) during August and September 2016. For Exp0 in August, low salinity
259 waters are found In the Beaufort Sea near the Mackenzie River and along the East Siberian
260 coast. In September, the low saline waters below 30 psu bridge the two areas in Exp0
261 probably due to sea ice melt, although the lowest salinity near the Siberian coast remains
262 unchanged from August to September (as indicated by the 28 psu isoline). Both in ExpV2
263 and ExpV3, the low salinity areas are even fresher during the two months compared to Exp0.
264 Notably, the areas of salinity lower than 28 psu are broader in ExpV3. On the European side
265 of the Arctic, the characteristics of the saline Atlantic water are very similar in all the three
266 runs (as shown by the isolines of 34 and 35 psu in Fig. 3). This is an indication that the
267 model ensemble has a lower standard deviation of SSS and thus less sensitivity to the SSS
268 assimilation in high salinity areas. Furthermore, clear salinity differences are observed in all
269 Arctic marginal seas. The relatively saline tongue in the northwest Laptev Sea indicated by
270 the 32 psu isoline is found in various locations in all three runs. In the Laptev Sea, due to the



271 significant effects of river runoff and ice melt, the salinity shows a strong gradient from the
272 southeast to the northern part. During winter, the salinity increases to 34 psu, and decreases
273 in summer near to 30 psu (Janout et al., 2017). In Exp0, the 32 psu salinity tongue extends
274 eastward to Taymyr Peninsula (TP). In ExpV2, the salinity tongue extends eastwards but is
275 narrower, but in ExpV3 it remains to the West of Severnaya Zemlya. North of the TP, the
276 Kara Sea freshwater meets with the Atlantic Water pathways from the Fram Strait and
277 Barents Sea (shown in Figure 1 of Janout et al., 2017). Close to TP, the observations at the
278 mooring profiles in Janout et al. (2017) show much fresher surface salinity (29 psu) than the
279 subsurface salinity (32 psu) in summer. This motivates the assimilation of the SSS products
280 to compensate for the paucity of in-situ observations.

281 The 32 psu isoline in ExpV3 extends hundreds of kilometers further South along east
282 Greenland in comparison to Exp0 and ExpV2. The change between simulations is larger
283 than the differences between August and September. Another area of notable differences is
284 in the northern Baffin Bay. In ExpV3, the area above 32 psu is shrunken to the South of
285 Nares Strait under the assimilation of the V3.1 SSS product, which may compensate for the
286 lack of mass loss from the Greenland ice sheet in the model.

287 In the above comparisons of SSS maps, the central Arctic is excluded, since the region is
288 covered by sea ice and the effect of assimilation can only be indirect.

289

290 *4.2 Comparison with independent in situ observations*

291 Valid observations in the Central Arctic are very unevenly distributed. When pooling all
292 observation types together, we further investigate the SSS misfits separated into six
293 subregions of the Arctic (Fig. 1 and Table 2). This section will present statistics of differences
294 to independent in situ observations considering marginal seas separately.

295

296 *Beaufort Sea:* Figure 4 shows the scatterplots of SSS in the three runs against in situ
297 observations which are respectively obtained from BGEP, OMG, and ICES. In the Beaufort
298 Sea (top panel in Fig. 4), the observed SSS varies in a range of 26-29 psu. The range of
299 SSS in Exp0 is much smaller, between 29-31 psu with a saline bias of 2.6 psu and an RMSD
300 of 2.7 psu, but otherwise show a reasonably linear relationship. The SSS bias in Exp0 has
301 the same value as in Xie et al. (2019), although estimated using the BGEP observations in a
302 different time period of 2011-2013. The range of SSS in ExpV2 is slightly improved to 28-
303 30.5 psu, a bias reduction by around 0.5 psu, corresponding to bias and RMSD reductions of
304 respectively 13.5% and 10.5% with respect to Exp0. In ExpV3, the SSS range is much
305 closer, between 26.5 and 30.5 psu, so the bias and RMSD reductions in ExpV3 are
306 respectively 26.3% and 17.3% with respect to Exp0. Furthermore, compared with the
307 combined SSS observations shown in the upper of Fig. 6, the SSS misfits in ExpV3 have a



308 robust reduction of 26.0% for bias and 20.6% for RMSD. There is also a reduction in ExpV2
309 of 13.5% for bias and 11.5% for RMSD, but smaller in comparison with ExpV3. These results
310 clearly indicate that assimilating the new version of the SSS is more efficient to improve the
311 SSS in the Beaufort Sea.

312

313 *Chukchi Sea:* Fig. 5 shows the SSS deviations as a function of time during the SKQ cruise
314 route. Relative to CTD observations, the SSS deviation in the runs are shown as the curves
315 in Fig. 5a. The saline bias (2.8 psu) is more pronounced than in the Beaufort Sea, for which
316 we blame to the climatology relaxation in the Bering Strait where the interannual variability of
317 the Pacific water is not included. After assimilating both SSS products, a gradual reduction of
318 the bias is observed during September, by 15.5% in ExpV2 and up to 22,2% in ExpV3. By
319 the meantime, the comparison to underway surface water samples (Fig. 5b) also shows the
320 error reductions errors around 15%, though less differences between V2 and V3.

321 Furthermore, compared with the combined SSS observations in CS (Fig. 6; bottom panels),
322 the SSS in Exp0 shows a very narrow varied range with a saline bias about 2.3 psu and the
323 RMSD 2.6 psu. A recent observational study by Goñi et al. (2021) shows that the surface
324 salinity of CS during late summer varies around 28-30 psu during 2016-2017 time period. In
325 our analysis for the year 2016, the SSS observations in the region vary around 27-32 psu.
326 through the assimilation of SSS products, the two runs of Exp V2 and ExpV3, show reduced
327 misfits (bias and RMSD). And as expected, the SSS in ExpV3 has more significant
328 reductions in bias (17.7%) and RMSD (16.4%). After assimilation, the deviations are in the
329 same range as found in the BS.

330

331 *Greenland Sea:* Around Greenland, most SSS observations are from OMG shown as the red
332 downward triangles in Fig. 1, distributed around both of the western and easter coastlines.
333 Firstly, compared with all SSS observations from OMG, the SSS misfits in the three runs
334 (shown in the middle panels of Fig. 4 show smaller bias and RMSD if relative to these values
335 in BS and CS. However, the SSS in ExpV3 still shows significant error reductions where the
336 saline bias/RMSD has a reduction of 32.6%/9.4% compared to that in Exp0. Notably, the
337 SSS misfits in ExpV2 are almost the same as in Exp0, which suggests that the V2.0 SSS
338 product loses the benefit around there by DA in this system.

339 To better understand the changes caused by the SSS assimilation and the potential
340 dependence on the localization, we further respectively evaluate the SSS deviations in GS
341 and BB where the involved observations are shown in Fig. 1 (also these two regions are
342 listed as S5 and S6 in Table 2). As shown in the top panel of Fig. 7, the SSS observations in
343 GS vary between 27 and 35 psu. This large SSS variation reflects the real condition: where
344 the fresh Arctic water and the fresh coast water converge with the saltier Atlantic Water. The



345 three assimilation runs show different saline biases, especially for salinities less than 30 psu.
346 While in observations the minimum salinity is lower than 28 psu, it is around 30 psu in
347 ExpV3, and 31 psu in Exp0 and ExpV2. Correspondingly, the bias reduction in ExpV3 is over
348 50% with the RMSD decreased about 10.5% in GS. Notably, no clear changes for SSS in
349 ExpV2 are found in comparison with Exp0. As indicated from SSS scatterplots of the three
350 runs in BB (S6 in Table 1, also shown in bottom panels of Fig. 7), there are no clear
351 differences between ExpV2 and Exp0 (less than 0.02 psu). On the other hand, w.r.t ExpV2
352 and Exp0, ExpV3 registers a reduction of the SSS bias, even has no significant reduction of
353 the RMSD in GS.

354

355 Next, we focus on the Barents Sea region (S3 in Table 2) and the Norwegian Sea (S4 in
356 Table 2). The SSS bias and RMSD are the lowest in ExpV3 in Table 2, even though the
357 reductions are not so significant as in the above basins. Compared to the ICES observations
358 distributed in the North Atlantic and extended in Nordic Seas (blue squares in Fig. 1), the
359 scatterplots of Exp0 and ExpV2 are almost similar in the bottom panels of Fig. 4. The
360 minimum salinity in these two runs is higher than 32 psu. The SSS bias and RMSD in both
361 runs are also similar (differences less than 0.01 psu). In contrast, lower saline values in
362 ExpV3, are below 32 psu, although the saline bias remains still around 0.5 psu on average.
363 Notably, the SSS in ExpV3 shows this assimilation brings a bias reduction of 15% compared
364 to Exp0, but the RMSD only reduced about 0.03 psu. It further suggests how to improve the
365 fresh salinity measurements near the coastline around the Nordic Seas will be the next
366 challenge for the SSS retrieve after the V3.1 SSS product.

367

368 *4.3 Impact analysis of the SSS assimilation*

369 Above quantitative validation of SSS against various observations, shows that the
370 assimilation of these two satellite products brings many positive benefits to constrain the
371 simulated SSS not too far from real conditions, although the improvements are quite
372 dependent on the locations. Surface salinity changes in the three runs (Fig. 8) contrasts the
373 averaged increment of SSS in 2016. The increment means the difference between the
374 analysis model state and the previous forecast model state, and represents the model
375 correction of SSS by DA. As a control reference, the SSS increment in Exp0 is mainly in the
376 river mouths, such as those around the Lena River (LR) and the Yenisey River (YR), while in
377 open ocean it is extremely small. This is an indication that the presently assimilated
378 observations in Exp0 are not able to correct the surface salinity very much. Assimilation of
379 version 2.0 SSS product (Fig. 8b) shows four dominant areas around the central Arctic with
380 negative increment in SSS. Two of them are in the Kara Sea (KS) and the East Siberian Sea
381 (ESS). These are regions where the model has an underestimation for the affected extent of



382 the freshwater impulse around rivers. The third region, the southern Laptev Sea (LS), is
383 found to be further separated into two small areas. The fourth region is along the coastline in
384 Beaufort Sea. On the contrary, a positive increment in SSS is found in the Hudson Bay (HB),
385 outside the central Arctic
386 In comparison to ExpV2, except for the wide negative SSS increment area around ESS,
387 much more areas are found with the different incremental patterns in ExpV3 (Fig. 8c). Two
388 strong positive SSS increment centers appear around the Kara Sea and the north of LS,
389 which is clearly different from the increment pattern in ExpV2. The difference is likely due to
390 the processing of the two versions of the SSS products using different climatologies
391 (Martínez et al., 2022). The two nearby regions (BS coast and HB) with negative SSS
392 increment regions in ExpV2 are found to form a dipole of negative and positive increment
393 regions in ExpV3. This pattern is likely due to the benefits of the increase in the horizontal
394 resolution in the newest version of SSS products. In addition, some regions with positive
395 increment (around 0.1 psu) are also visualized in Fig. 8c, significantly different to that in
396 Exp0: region extending from south of Fram Strait and to north of Denmark Strait; northern
397 Baffin Bay; Chukchi Sea shelf. These spatial features of positive and negative SSS
398 increments in ExpV3 indicate the impact of DA in the Arctic basins. On the other hand, the
399 Barents Sea, Norwegian Sea, and the north Atlantic don't show significant changes due to
400 the SSS assimilation for both runs, which is also consistent with the SSS scatterplots shown
401 in Fig. 4 (bottom panels).

402

403 Since the water salinity near the surface are changed by the SSS DA, it is natural to further
404 investigate how big the impact on the freshwater in the Arctic Ocean. Based on these
405 assimilation runs, the changes in the Freshwater Content (FWC) in the Arctic are calculated
406 according to the method by Proshutinsky et al. (2009), although this method was proposed
407 initially to diagnose the FWC anomalies in the BS:

$$408 \quad FWCL = \int_{z_2}^{z_1} \frac{[S_{ref} - S_z]}{S_{ref}} dz \quad (6)$$

409 Where the reference salinity value S_{ref} is taken at 34.8 psu and the vertical integral is
410 computed from surface on all the waters fresher than S_{ref} . Recently, applying the same
411 methodology on optimized interpolation on the collected in-situ observations, Proshutinsky et
412 al. (2020) estimated the time-averaged summer freshwater content in the Beaufort Gyre
413 region for two time-period (1950s-1980s and 2013-2018). They show the FWC centre in BS
414 is located around (150°W, 75°N) and the 20-m isoline covers more than 5 degrees of latitude
415 and nearly 30 degrees of longitude on average. During the recent years (2013-2018), the
416 FWC in BS has an obvious increase compared with before and its centre has a westward
417 shift.



418 Correspondingly, referring to Eq. 6, the FWC of the water column has been computed from
419 surface until the depth reaching to 34.8 psu. Figure 9 shows the FWC around the Arctic on
420 20th September and 20th October 2016, respectively. In Exp0, the reanalysis reproduces the
421 FWC spread in the Arctic region and a dominant centre located in the Beaufort Sea. Tracking
422 of the 20 m FWCL isolines in Fig. 9a and 9d, it shows an increase in its spatial coverage
423 during October, which verifies the variability due to winds, sea ice conditions, and ocean
424 mixing processes. After assimilation of the V2.0 SSS product, the FWC spatial maximum in
425 BS is found to show a different distribution in Fig. 9b and 9e in comparison to that in Exp0.
426 An increase in FWC is noted outside the BS, north of Canada (indicated by the 16-m isoline).
427 Another noticeable change is the FWCL extending (shown as the 8-m isoline) along the East
428 Siberian shelf and near the coast in the Laptev Sea (LS). It indicates that the SSS
429 assimilation is able to correct the possible fresh bias related to the river fluxes in the model
430 near the coastal regions in ESS and LS. In ExpV3, the FWC on the shelf region of ESS is
431 higher compared to that in ExpV2, but lower near the southwest coast of LS. These results
432 suggest that the SSS assimilation of both versions of satellite products will redistribute the
433 freshwater in the Arctic, and the freshwater budget will be adjusted in the end. However, so
434 far with the limited amount of in-situ data, it is not fair to conclude whether this is a change
435 for the better or the worse. Significantly different from sparse in-situ observations in the
436 Arctic, the reanalysis product can better represent the characteristics of FWC variations in
437 space and time.

438 Further, we intercompare the daily time series of FWCL from the three runs averaged over
439 north of 70°N (Fig. 10). The averaged FWCL clearly shows a sharp increase till October-
440 November to reach the maximum, and gradually decreases thereafter. The impact of weekly
441 data assimilation cycles is visible as instantaneous jumps on the three curves of the time
442 series. The summer FWC is found to increase substantially due to SSS assimilations in
443 ExpV2 and ExpV3. Notably the assimilation of version 3.1 SSS brings faster increase during
444 the first two months. Since there is not enough ground truth data in 2016, the above
445 comparison can only be qualitative, but the timing is in better agreement with the ITP data
446 presented by Rosenblum et al. (2021, their Fig. 4), although the amplitude of the seasonal
447 FWC seems too small in all experiments, which can be related to insufficient thick ice in
448 TOPAZ4 (Uotila et al., 2019). More concrete evidence about the changed FWC will be
449 provided, after when the longer assimilation of the satellite-based SSS product is finished in
450 near future.

451

452 **5. Summary and discussions.**



453 SSS plays a key role to track the water property in the global water cycle and the ocean
454 dynamics, but hindered by the extreme paucity of in situ data, the Arctic SSS still has high
455 uncertainty. As a promising tool to measure the SSS changes in Arctic at basin scale, the
456 grided SSS products from SMOS undoubtedly provide a way constraining the salinity
457 deviations, especially for the ocean forecast systems. However, due to the limits of the
458 previous SSS products, there have not been any previous studies to investigate the real
459 benefits or challenges for assimilation of SMOS SSS in the Arctic reanalysis. In this study,
460 based on the coupled ice-ocean data assimilative system, three assimilation runs have done.
461 Exp0 assimilated all available altimeter data, SST, sea ice concentration, sea ice drift, T/S
462 profiles, sea ice thickness, except any SMOS SSS products. ExpV2 and ExpV3 additionally
463 assimilated V2.0 and V3.1 of SSS products from BEC, which were tested and retrieved by a
464 series of algorithms considering the low temperature and sea ice cover in the Arctic (Olmedo
465 et al., 2017; Martínez et al., 2022).

466 Evaluated by the independent SSS observations from CTD and surface water samples along
467 the cruise underway, the quantitative misfits in ExpV2 and ExpV3 have been significantly
468 reduced relative to that in Exp0. In the Beaufort Sea, the SSS bias and RMSD in ExpV3 is
469 reduced respectively by 26.0% and 20.6%, and if validated only against the observations
470 from BGEP, the reduction is up to 26.3% and 17.3% respectively (Fig. 4). For ExpV2, the
471 RMSD is reduced by 11.5% (if validated against the BGEP CTD profiles about 10.5% in Fig.
472 4). In the Chukchi Sea, the reduction in SSS misfits in ExpV3 (bias:17.7%; RMSD: 16.4%) is
473 more than that in ExpV2 (bias: 15.5%; RMSD: 13.7%). Around Greenland, validated by the
474 SSS observations from OMG, a significant reduction in the SSS bias (32.6%) and RMSD
475 (9.4%) is found in ExpV3, while there is no notable improvement in ExpV2. Furthermore,
476 dividing the observations around Greenland into two regions, S5 and S6 (Table 2 and Fig. 7)
477 show a larger reduction in the bias (52%) and RMSD (10.5%) in the Greenland Sea (S5) in
478 ExpV3 SSS relative to that in Exp0. Notably in the Baffin Bay (S6), only the SSS bias in
479 ExpV3 shows an obvious reduction compared with Exp0. It is consistent with the markable
480 adjustment along the 34 psu isoline near the ice edge in GS (shown in Fig. 3). Increments of
481 SSS (in Fig. 8) also clearly show the wide salty features located in the GS in ExpV3, which is
482 clearly different to that in Exp0 and ExpV2. In addition, the increments for other variables
483 such as SST, SIC and so on are diagnosed, but their spatial features during the same time
484 (figures not shown) have no clear differences as in Exp0. It further verifies the surface salinity
485 is dominantly constrained by the direct observations from SMOS, other than the weak
486 constraints through the error covariance from other observed variables. This finding also is
487 consistent with the conclusions in SSS assimilation experiments in the tropics (Chakraborty
488 et al.,2015; Tranchant et al.,2019).

489



490 Furthermore, this study shows that the error reduction of SSS will be benefited from the
491 assimilation of the V3.1 product from SMOS, even outside of the central Arctic. A remarkable
492 improvement is also achieved around GS (S5 in Fig. 1), a clear advantage compared to the
493 other version of SSS product. Moreover, our analysis shows different spatial distributions of
494 Arctic FWC as a result from assimilating the two SMOS products respectively. The mean
495 FWCL north of 70°N shows that the FWC in the whole central Arctic can be corrected by the
496 SSS innovations though DA, although the FWCL time series shows a clear step jump for
497 each assimilation cycle. Assimilation experiments show that the Arctic FWC can be
498 redistributed by assimilation, but how the seasonal cycle varies with time still needs a longer
499 assimilation time. Clearly, these novel results are not only useful for the developing of the
500 Arctic reanalysis and the operational ocean forecast system, but also provides insights for
501 understanding the differences of these two SSS products although they have a certain
502 degree of similarity. These results are also expected to guide the future upgrade of the SSS
503 products.

504

505 Using the quantitative SSS misfits (Table 2), the impact indexes at each subregion (S1 to S6)
506 further indicates whether the misfits are significantly decreased or not. Outside of the central
507 Arctic, the v2.0 SSS product loses the impacts in this system, but the V3.1 SSS brings more
508 wider significant impacts around the Arctic, which clearly benefits from the related retrieval
509 algorithms for the refined effective resolution (Martínez et al., 2022). However, in the region
510 S6, the SSS in ExpV3 has no significant constraint on the misfits and only brings a reduction
511 in the bias. It may be related with the movement of the sea ice edge more northward in
512 summer and indicates that both the SSS products have low impacts over the open water in
513 the north Atlantic. It is also verified by the validation results in the Barents Sea and the
514 Norwegian Sea, as shown in bottom panels of Fig. 4 and Table 2. This defect partly reflects
515 the mesoscale eddy features (<50 km which is about 4 times the model resolution in
516 TOPAZ4) having no clear benefits from this assimilation using the 9-days SSS. In fact, the
517 V3.1 SSS also provides a 3-days product that needs to be tested by DA for quantifying the
518 impact on the north Atlantic. Meanwhile, considering the coarse footprint of the SMOS
519 radiometer (about 40 km in diameter), minimal sampling densities (e.g., Lv et al., 2020) is
520 required to resolve the mesoscale eddy features. But in real conditions the gridded SSS
521 products still have a gap for more precisely measuring the SSS changes near the Nordic
522 coast regions. Using the same L-band frequency (e.g., Lee et al, 2012), Aquarius used three
523 radiometers at fixed angles and had a 350 km wide swath that covered earth's surface in
524 seven days. Whereas SMAP scans earth using a spinning antenna, with a wider swath about
525 1000 km every three days to provide global coverage (e.g., Tang et al., 2017; Reul et al.,
526 2020). To combine all the SSS retrieves along the satellite tracks will provide the



527 contemporaneous data coverage with the greatest extent, which should be helpful in Arctic
528 and high-latitudes for further improvements of the reanalysis and the ocean forecasting.
529

530 **Data availability.** All the in situ observations for validation in this study are open accessed
531 as the states in Sect. 3. The model result in Exp0 same as the released reanalysis from
532 TOPAZ4 which is freely available from CMEMS (<http://marine.copernicus.eu>). Other two
533 assimilation data can be freely provided for public by personal communication.

534

535 **Author contributions.** JX initiated the design and carry of the assimilation experiments.
536 LB and RR contributed the result interpretation. JC collected the SSS data. CG and RC
537 enhanced the understanding for the uncertainty of the satellite data. All the authors
538 contribute to edit and correct this paper.

539

540 **Competing interests.** The authors declare that they have no conflict of interest.

541

542 **Acknowledgments:**

543 Thanks to the profile data providers: the OMG mission for the released final CTD data via
544 the [Physical Oceanography DAAC \(PO.DAAC\)](#); the ICES data portal (<https://www.ices.dk>);
545 the Arctic Data Center (<https://arcticdata.io/catalog/data>); and the BGEP data were available
546 based at the Woods Hole Oceanographic Institution
547 (<https://www2.whoi.edu/site/beaufortgyre/>) in collaboration with researchers from Fisheries
548 and Oceans Canada at the Institute of Ocean Sciences. This study has been supported by
549 the ESA Arctic Salinity+ project and by the NFR Thickness of Arctic sea ice Reconstructed
550 by Data assimilation and artificial Intelligence Seamlessly (TARDIS) project. The computation
551 of the assimilation experiments and the plotting of the results were performed on resources
552 provided by Sigma2-the National Infrastructure for High Performance Computing and Data
553 Storage in Norway with the projects of nn2293k and nn9481k and the relevant store space
554 under the projects of ns9481k and ns2993k.

555

556 **Reference:**

557 Bouillon, S., Fichefet, T., Legat, V., and Madec, G.: The elastic-viscous-plastic method revised,
558 *Ocean Modell.*, 7, 2–12, <https://doi.org/10.1016/j.ocemod.2013.05.013>, 2013.



- 559 Boutin J., Vergely J.-L., and Khvorostyanov D.: SMOS SSS L3 maps generated by CATDS
560 GEC LOCEAN. debias V7.0. SEANOE. <https://doi.org/10.17882/52804#91742>, 2022.
- 561 Boyer, T. P., Levitus, S., Antonov, J. I., Locarnini, R. A., and Garcia, H. E.: Linear trends in
562 salinity for the World Ocean, 1955–1998, *Geophys. Res. Lett.*, 32, L01604,
563 doi:[10.1029/2004GL021791](https://doi.org/10.1029/2004GL021791), 2005.
- 564 Carmack, E. C., Yamamoto Kawai, M., Haine, T. W. N., Bacon, S., Bluhm, B. A., Lique, C.,
565 Melling, H., Polyakov, I. V., Straneo, F., Timmermans, M.-L., and Williams, W. J.:
566 Freshwater and its role in the Arctic Marine System: Sources, disposition, storage, export,
567 and physical and biogeochemical consequences in the Arctic and global oceans, *J. Geophys. Res.-Biogeo.*, 121, 675–717, <https://doi.org/10.1002/2015JG003140>, 2016.
- 569 Chakraborty, A., Sharma, R., Kumar, R., and Basu, S.: Joint Assimilation of Aquarius-derived
570 Sea Surface Salinity and AVHRR-derived Sea Surface Temperature in an Ocean General
571 Circulation Model Using SEEK Filter: Implication for Mixed Layer Depth and Barrier Layer
572 Thickness, *J. Geophys. Res.-Oceans*, 120 (10), 6927–6942, doi: 10.1002/2015JC010934,
573 2015.
- 574 Chassignet, E. P., Smith, L. T., and Halliwell, G. R.: North Atlantic Simulations with the Hybrid
575 Coordinate Ocean Model (HYCOM): Impact of the vertical coordinate choice, reference
576 pressure, and thermobaricity, *J. Phys. Oceanogr.*, 33, 2504–2526, doi:10.1175/1520-
577 0485(2003)033<2504:NASWTH<2.0.CO;2, 2003.
- 578 Cooper, L. W., Grebeier, J. M., Frey, K. E., and Vaglem, S.: Discrete water samples collected
579 from the Conductivity-Temperature-Depth rosette at specific depths, Northern Bering Sea
580 to Chukchi Sea, 2016. Arctic Data Center. [doi:10.18739/A23B5W875](https://doi.org/10.18739/A23B5W875), 2019.
- 581 Curry, R., Dickson, R., and Yashayaev, I.: A change in the freshwater balance of the Atlantic
582 Ocean over the past four decades, *Nature*, 426, 826–829, doi:[10.1038/nature02206](https://doi.org/10.1038/nature02206), 2003.
- 583 Dombrowsky, E., Bertino, L., Cummings, J., Brassington, G. B., Chassignet, E. P., Davidson,
584 F., ... Tonani, M. (2009). GODAE systems in operations. *Oceanography*, 22(3), 80–95.
585 <https://doi.org/10.5670/oceanog.2009.68>
- 586 Drange, H. and Simonsen, K.: Formulation of air-sea fluxes in the ESOP2 version of MICOM,
587 Technical Report No. 125, Nansen Environmental and Remote Sensing Center, 23 pp.,
588 1996.
- 589 Evensen, G.: The ensemble Kalman filter: theoretical formulation and practical
590 implementation, *Ocean Dynam.*, 53, 343–367, doi:10.1007/s10236-003-0036-9, 2003
- 591 Fenty, I., Willis, J. K., Khazendar, A., Dinardo, S., Forsberg, R., Fukumori, I., Holland, D.,
592 Jakobsson, M., Moller, D., Morison, J., Meuncho, A., Rignot, E., Schodlock, M.,
593 Thompson, A.F., Tino, K., Rutherford, M., and Trenholm, N.: Oceans Melting Greenland:
594 Early results from NASA's ocean-ice mission in Greenland. *Oceanography* 29(4):72-83,
595 <https://doi.org/10.5670/ocean.2016.100>, 2016.



- 596 Font, J., Camps, A., Borges, A., Martín-Neira, M., Boutin, J., Reul, N., Kerr, Y. H., Hahne, A.,
597 and Mecklenburg, S.: SMOS: The challenging sea surface salinity measurement from
598 space, *Proc. IEEE*, 98(5), 649–665, DOI: [10.1109/JPROC.2009.2033096](https://doi.org/10.1109/JPROC.2009.2033096), 2010.
- 599 Fujii, Y., Rémy, E., Zuo, H., Oke, P., Halliwell, G., Gasparin, F., et al.: Observing system
600 evaluation based on ocean data assimilation and prediction systems: on-going challenges
601 and a future vision for designing and supporting ocean observational networks. *Front. Mar.*
602 *Sci.* 6:417. doi: 10.3389/fmars.2019.00417, 2019.
- 603 Goñi, M. A., Corvi, E. R., Welch, K. A., Buktenica, M., Lebon, K., Alleau, Y., and Juranek, L.
604 W.: Particulate organic matter distributions in surface waters of the Pacific Arctic shelf
605 during the late summer and fall season. *Marine Chemistry*, 211, 75-93,
606 doi:10.1016/j.marchem.2019.03.010, 2019.
- 607 Goñi, M. A., Juranek, L. W., Sipler, R. E., and Welch, K. A.: Particulate organic matter
608 distributions in the water column of the Chukchi Sea during late summer. *Journal of*
609 *Geophysical Research: Oceans*, 126(9), doi:10.1029/2021JC017664, 2021.
- 610 Janout, M. A., J. Hölemann, L. Timokhov, O. Gutjahr, and G. Heinemann: Circulation in the
611 northwest Laptev Sea in the eastern Arctic Ocean: Crossroads between Siberian River
612 water, Atlantic water and polynya-formed dense water, *J. Geophys. Res. Oceans*, 122,
613 6630–6647, doi:10.1002/2017JC013159, 2017.
- 614 Johannessen, O. M., Shalina, E. V., and Miles, M. W.: Satellite evidence for an Arctic Sea
615 ice cover in transformation, *Science*, 286, 1937–1939,
616 <https://doi.org/10.1126/science.286.5446.1937>, 1999.
- 617 Kaminski, T., Kauker, F., Eicken, H., & Karcher, M. (2015). Exploring the utility of quantitative
618 network design in evaluating Arctic sea ice thickness sampling strategies. *Cryosphere*,
619 9(4), 1721–1733. <https://doi.org/10.5194/tc-9-1721-2015>
- 620 Kerr, Y. H., Waldteufel, P., Wigneron, J. P., Delwart, S., Cabot, F., Boutin, J., Escorihuela, M.
621 J., Font, J., Reul, N., Gruhier, C., Juglea, S., Drinkwater, M. R., Hahne, A., Martín-Neira,
622 M., and Mecklenburg, S.: The SMOS mission: New tool for monitoring key elements of the
623 global water cycle, *Proc. IEEE*, 98(5), 666–687, doi:[10.1109/JPROC.2010.2043032](https://doi.org/10.1109/JPROC.2010.2043032), 2010.
- 624 Lee, T., Lagerloef, G., Gierach, M. M., Kao, H. -Y., Yueh, S. S., and Dohan, K.: Aquarius
625 reveals salinity structure of tropical instability waves. *Geophys. Res. Lett.*, 39, L12610,
626 doi:10.1029/2012GL052232, 2012.
- 627 Lu, Z., Cheng, L., Zhu, J., and Lin, R.: The complementary role of SMOS sea surface salinity
628 observations for estimating global ocean salinity state, *J. Geophys. Res. Oceans*,
629 121,doi:10.1002/2015JC011480, 2016.
- 630 Lv, S., Schalge, B., Saavedra Garfias, P., and Simmer, C.: Required sampling density of
631 ground-based soil moisture and brightness temperature observations for calibration and



- 632 validation of L-band satellite observations based on a virtual reality, *Hydrol. Earth Syst. Sci.*,
633 24, 1957–1973, <https://doi.org/10.5194/hess-24-1957-2020>, 2020.
- 634 Martin, M. J., King, R. R., While, J., Aguiar, A. B.: Assimilating satellite sea-surface salinity
635 data from SMOS, Aquarius and SMAP into a global ocean forecasting system. *Quarterly*
636 *Journal of the Royal Meteorological Society*, 145(719), 705-726, doi:10.1002/qj.3461,
637 2019.
- 638 Martínez, J., Gabarró, C., and Turiel, A.: Algorithm Theoretical Basis Document, Arctic+Salinity
639 ITT, Tech. rep., BEC, Institut de Ciències del Mar-CSIC,
640 <https://doi.org/10.13140/RG.2.2.12195.58401>, 2020.
- 641 Martínez, J., Gabarró, C., Turiel, A., González-Gambau, V., Umberto, M., Hoareau, N.,
642 González-Haro, C., Olmedo, E., Arias, M., Catany, R., Bertino, L., Raj, R. P., Xie, J., Sabia,
643 R., and Fernández, D.: Improved BEC SMOS Arctic Sea Surface Salinity product v3.1,
644 *Earth Syst. Sci. Data*, 14, 307–323, <https://doi.org/10.5194/essd-14-307-2022>, 2022.
- 645 Olmedo, E., Martínez, J., Turiel, A., Ballabrera-Poy, J., and Portabella, M.: Debaised non-
646 Bayesian retrieval: A novel approach to SMOS Sea Surface Salinity, *Remote Sens.*
647 *Environ.*, 193, 103– 126, <https://doi.org/10.1016/j.rse.2017.02.023>, 2017.
- 648 Olmedo, E., Gabarró, C., González-Gambau, V., Martínez, J., Ballabrera-Poy, J., Turiel, A.,
649 Portabella, M., Fournier, S., and Lee, T.: Seven Years of SMOS Sea Surface Salinity at
650 High Latitudes: Variability in Arctic and Sub-Arctic Regions. *Remote Sensing*. 2018;
651 10(11):1772, <https://doi.org/10.3390/rs10111772>, 2018.
- 652 Proshutinsky, A., Krishfield, Timmermans, M.-L., Toole, J., Carmack, E., Mclaughlin, F.,
653 Williams, W. J., Zimmermann, S., Itoh, M., and Shimada, K.: Beaufort Gyre freshwater
654 reservoir: State and variability from observations, *Journal of Geophysical Research*, 114,
655 1–25, doi:10.1029/2008JC005104, 2009.
- 656 Proshutinsky, A., Krishfield, R., and Timmermans, M.-L.: Introduction to special collection on
657 arctic ocean modeling and observational synthesis (FAMOS) 2: beaufort gyre phenomenon.
658 *Journal of Geophysical Research: Oceans*, 125, e2019JC015400. [https://doi.org/](https://doi.org/10.1029/2019JC015400)
659 [10.1029/2019JC015400](https://doi.org/10.1029/2019JC015400), 2020.
- 660 Reul, N., Grodsky, S., Arias, M., Boutin, J., Catany, R., Chapron, B., D’Amico, F., Dinnat, E.,
661 Donlon, C., Fore, A., Fournier, S., Guimbar, S., Hasson, A., Kolodziejczyk, N., Lagerloef,
662 G., Lee, T., Le Vine, D., Lindstrom, E., Maes, C., Mecklenburg, S., Meissner, T., Olmedo,
663 E., Sabia, R., Tenerelli, J., Thouvenin-Masson, C., Turiel, A., Vergely, J., Vinogradova, N.,
664 Wentz, F., and Yueh, S.: Sea surface salinity estimates from spaceborne L-band
665 radiometers: An overview of the first decade of observation (2010–2019), *Remote Sens.*
666 *Environ.*, 242, 111769, <https://doi.org/10.1016/j.rse.2020.111769>, 2020.
- 667 Rosenblum, E., Fajber, R., Stroeve, J. C., Gille, S. T., Tremblay, L. B., & Carmack, E. C.
668 (2021). Surface salinity under transitioning ice cover in the Canada Basin: Climate model



- 669 biases linked to vertical distribution of fresh water. *Geophysical Research Letters*, 48,
670 e2021GL094739. <https://doi.org/10.1029/2021GL094739>
- 671 Sakov, P., Counillon, F., Bertino, L., Lisæter, K. A., Oke, P. R., and Korablev, A.: TOPAZ4: an
672 ocean-sea ice data assimilation sys- tem for the North Atlantic and Arctic, *Ocean Sci.*, 8,
673 633–656, <https://doi.org/10.5194/os-8-633-2012>, 2012.
- 674 Solomon, A., Heuzé, C., Rabe, B., Bacon, S., Bertino, L., Heimbach, P., ... Tang, H. (2021).
675 Freshwater in the Arctic Ocean 2010-2019. *Ocean Science*, 17(4), 1081–1102.
676 <https://doi.org/10.5194/os-17-1081-2021>
- 677 Steele, M., Morley, R., and Ermold, W.: PHC: A global ocean hydrography with a high-quality
678 Arctic Ocean, *J. Climate*, 14, 2079–2087, 2001.
- 679 Storto, A., Alvera-Azcárate, A., Balmaseda, M. A., Barth, A., Chevallier, M., Counillon, F.,
680 Domingues, C. M., Drevillon, M., Drillet, Y., Forget, G., Garric, G., Haines, K., Hernandez,
681 F., Iovino, D., Jackson, L. C., Lellouche, J.-M., Masina, S., Mayer, M., Oke, P. R., Penny, S.
682 G., Peterson, K. A., Yang, C. and Zuo, H.: Ocean Reanalyses: Recent Advances and
683 Unsolved Challenges. *Front. Mar. Sci.*, 6(418), doi: 10.3389/fmars.2019.00418, 2019.
- 684 Stroeve, J. and Notz, D.: Changing state of Arctic sea ice across all seasons, *Environ. Res.*
685 *Let.*, 13, 103001, <https://doi.org/10.1088/1748-9326/aade56>, 2018.
- 686 Stroh, J. N., Panteleev, G., Kirillov, S., Makhotin, M., and Shakhova, N.: Sea-surface
687 temperature and salinity product comparison against external in situ data in the Arctic
688 Ocean. *J. Geophys. Res.-Oceans*, **120**, 7223-7236,
689 <https://doi.org/10.1002/2015JC011005>, 2015.
- 690 Supply, A., Boutin, J., Vergely, J. L., Kolodziejczyk, N., Reverdin, G., Reul, N., & Tarasenko,
691 A. (2020). New insights into SMOS sea surface salinity retrievals in the Arctic Ocean.
692 *Remote Sensing of Environment*, 249, 112027. <https://doi.org/10.1016/J.RSE.2020.112027>
- 693 Tang, W., Fore, A., Yueh, S., Lee, T., Hayashi, A., Sanchez-Franks, A., Martinez, J., King, B.,
694 and Baranowski, D.: Validating SMAP SSS with in situ measurements, *Remote Sens.*
695 *Environ.*, 200, 326–340, <https://doi.org/10.1016/j.rse.2017.08.021>, 2017.
- 696 Tranchant, B., Remy, E., Greiner, E., and Legalloudec, O.: Data assimilation of Soil Moisture
697 and Ocean Salinity (SMOS) observations into the Mercator Ocean operational system:
698 focus on the El Niño 2015 event, *Ocean Sci.*, 15, 543–563, <https://doi.org/10.5194/os-15-543-2019>, 2019.
- 700 Uotila, P., Goose, H., Haines, K., Chevallier, M., Barthélemy, A., Bricaud, C., Carton, J.,
701 Fućkar, N., Garric, G., Iovino, D., Kauker, F., Korhonen, M., Lien, V. S., Marnela, M.,
702 Massonnet, F., Mignac, D., Peterson, A., Sadikn, R., Shi, L., Tietsche, S., Toyoda, T., Xie,
703 J., and Zhang, Z.: An assessment of ten ocean reanalyses in the polar regions, *Clim.*
704 *Dynam.*, 52, 1613–1650. <https://doi.org/10.1007/s00382-018-4242-z>, 2019.



- 705 Vinogradova, N.T., Ponte, R.M., Fukumori, I. and Wang, O. (2014) Estimating satellite salinity
706 errors for assimilation of Aquarius and SMOS data into climate models. *Journal of*
707 *Geophysical Research: Oceans*, 119(8), 4732–4744.
708 <https://doi.org/10.1002/2014JC009906>, 2014
- 709 Woodgate, R. A., Weingartner, T. J., and Lindsay, R.: Observed increases in Bering Strait
710 oceanic fluxes from the Pacific to the Arctic from 2001 to 2011 and their impacts on the Arctic
711 Ocean water column. *Geophys. Res. Lett.*, 39, L24603, doi:10.1029/2012GL054092, 2012.
- 712 Xie, J., Bertino, L., Counillon, F., Lisæter, K. A., and Sakov, P.: Quality assessment of the
713 TOPAZ4 reanalysis in the Arctic over the period 1991–2013. *Ocean Science*, 13(1). doi:
714 10.5194/os-13-123-2017, 2017.
- 715 Xie, J., Counillon, F., and Bertino, L.: Impact of assimilating a merged sea-ice thickness from
716 CryoSat-2 and SMOS in the Arctic reanalysis. *The Cryosphere*, 12(11), 3671–3691. doi:
717 10.5194/tc-12-3671-2018, 2018.
- 718 Xie, J., Raj, R. P., Bertino, L., Samuelsen, A., and Wakamatsu, T.: Evaluation of Arctic Ocean
719 surface salinities from the Soil Moisture and Ocean Salinity (SMOS) mission against a
720 regional reanalysis and in situ data, *Ocean Sci.*, 15, 1191–1206, [https://doi.org/10.5194/os-](https://doi.org/10.5194/os-15-1191-2019)
721 15-1191-2019, 2019.
- 722 Yu, L.: A global relationship between the ocean water cycle and near-surface salinity, *J.*
723 *Geophys. Res.*, 116, C10025, <https://doi.org/10.1029/2010JC006937>, 2011.
- 724 Yu, L., Jin, X., Josey, S. A., Lee, T., Kumar, A., Wen, C., and Xue, Y.: The Global Ocean Water
725 Cycle in Atmospheric Reanalysis, Satellite, and Ocean Salinity, *Journal of Climate*, 30(10),
726 3829–3852, 2017
- 727 Yueh, S., West, R., Wilson, W., Li, F., Nghiem, S., and Rahmat-Samii, Y.: Error Sources and
728 Feasibility for Microwave Remote Sensing of Ocean Surface Salinity, *IEEE T. Geosci.*
729 *Remote*, 39, 1049–1059, 2001.
- 730 Zweng, M. M., Reagan, J. R., Antonov J. I., Locarnini, R. A., Mishonov, A. V., Boyer, T. P.,
731 Garcia, H. E., Baranova, O. K., Johnson, D. R., Seidov, D., and Biddle, M. M.: World Ocean
732 Atlas 2013, Volume 2: Salinity, Levitus, S. (Ed.), Mishonov, A., Technical Ed. NOAA Atlas
733 NESDIS 74, 39pp, 2013.



Caption and figures:

Table 1. Settings of the three assimilation runs in 2016 with and without SSS.

	Assimilated obs.	Initial model states	End date of assimilation	SSS Observation Errors
Exp0	SST, SLA, T/S profile, SIC, SIT, and SID	6 th July	28 th Dec.	N/A
ExpV2	SSS V2.0 + obs. used in Exp0	6 th July	28 th Dec.	Eq. 3
ExpV3	SSS V3.1 + obs. used in Exp0	6 th July	28 th Dec.	Eq. 3

Table 2. Evaluation of SSS misfits (unit: psu) in the three assimilation runs according to the 6 sub-regions indicated by the blue dashed lines in Fig. 1. The bold fonts indicate the minimal misfits in the runs with a significant reduction (> 9% with respect to Exp0). The overall score is defined by whether the reductions of bias and RMSD are significant or not. If both reductions are significant, the index equals 1, but 2 if only one of them is reduced, and otherwise equals 3.

Region	Areas in Fig. 1	Number of obs.	Bias (psu)			RMSD (psu)			Overall score	
			Exp0	ExpV2	ExpV3	Exp0	ExpV2	ExpV3	ExpV2	ExpV3
S1	BS	98	2.81	2.43	2.08	2.87	2.54	2.28	1	1
S2	CS	137	2.32	1.96	1.91	2.62	2.26	2.19	1	1
S3	BSS	189	1.35	1.34	1.30	2.50	2.49	2.47	3	3
S4	NS	669	0.43	0.44	0.37	1.19	1.19	1.16	3	2
S5	GS	254	0.50	0.51	0.24	1.43	1.43	1.28	3	1
S6	BB	89	0.35	0.37	0.12	1.22	1.20	1.22	3	2

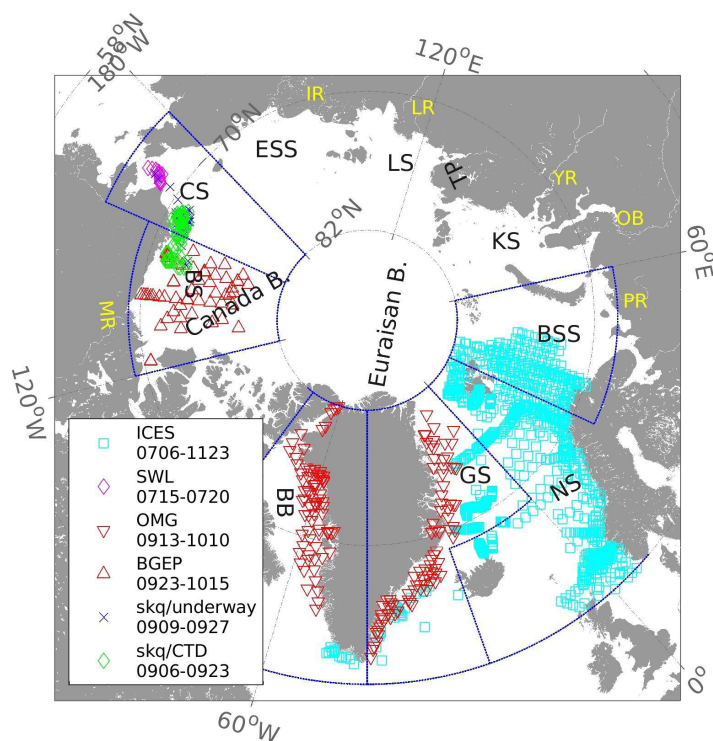


Fig. 1 Locations of the observed SSS from in-situ profiles and surface samples by cruises from July to December 2016. There are 6 observation sources noted by the marks, see the details in Section 2.3. The marginal seas delineated are the Beaufort Sea (BS), Chukchi Sea (CS), East Siberian Sea (ESS), Laptev Sea (LS), Kara Sea (KS), Barents Sea (BSS), Greenland Sea (GS), Norwegian Sea (NS), and Baffin Bay (BB). The main rivers around the Arctic region are the Mackenzie River (MR), Pechora (PR), the Ob (OB), Yenisey River (YR), Lena River (LR), and Indigirka River (IR). TP indicates the Taymyr Peninsula.

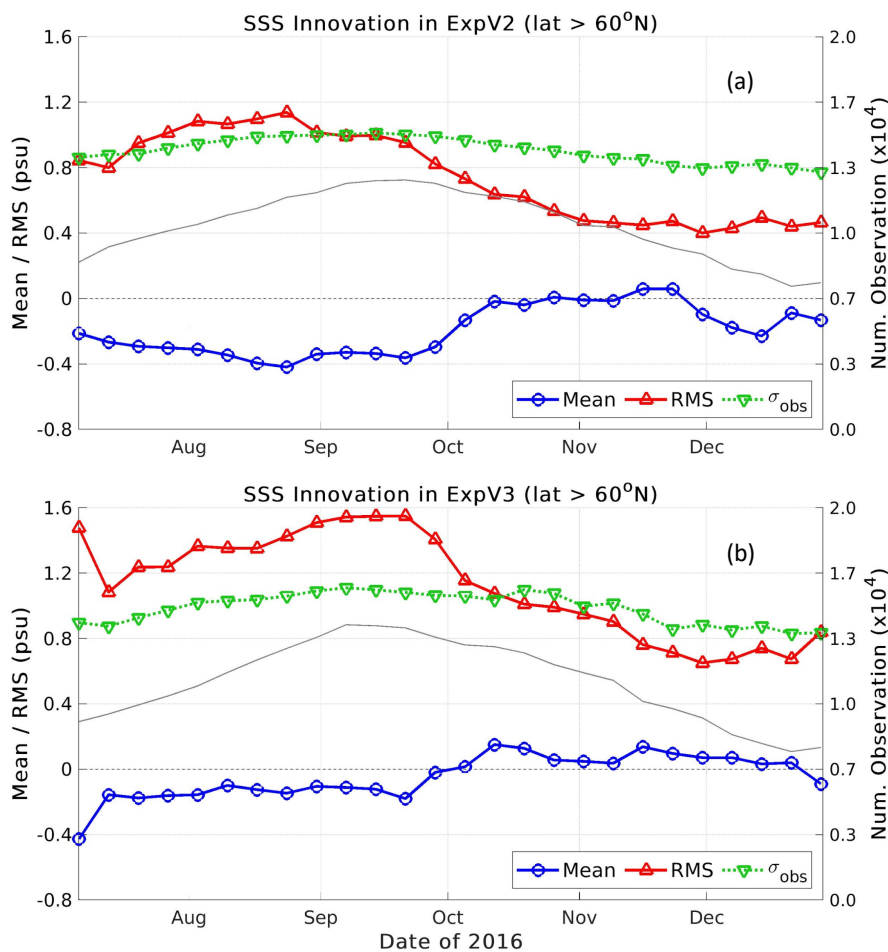


Fig 2. Innovations of SSS in both weekly assimilation runs ExpV2 (a) and ExpV3 (b).

The line with red triangles is the root mean squared innovation, and the blue dotted line shows the mean of innovations north of 60°N. The gray line represents the number of observations assimilated, and the line with inverted triangles is the observation error standard deviation in the two runs.

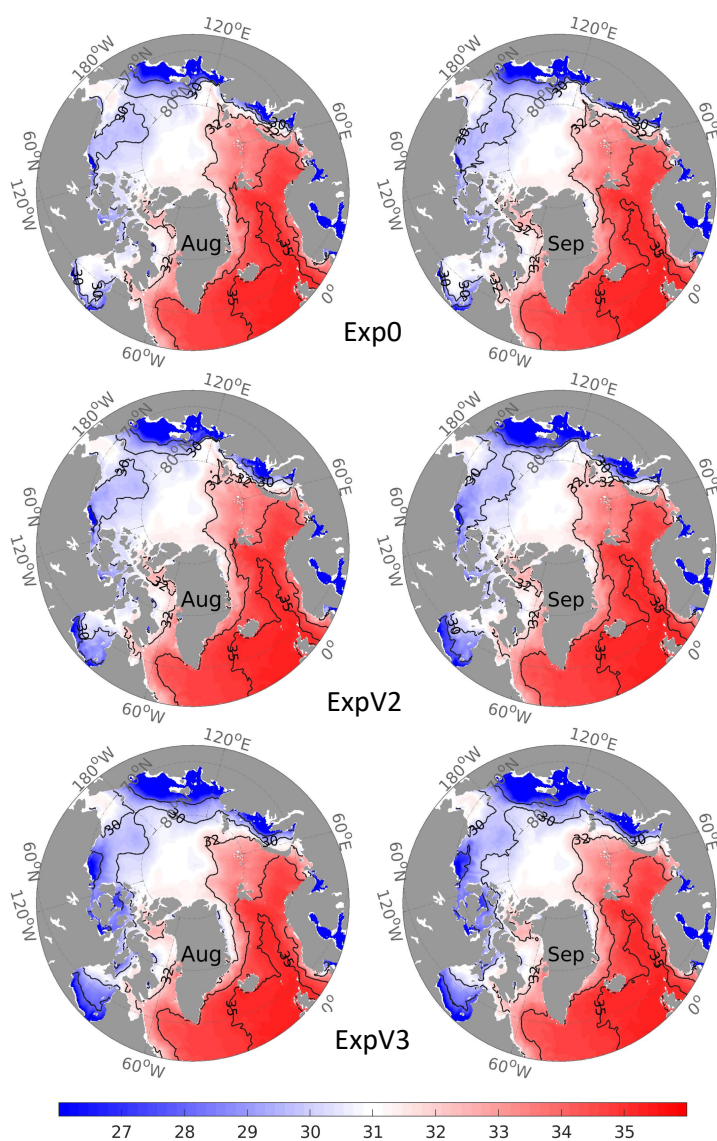


Fig. 3 Monthly simulated SSS (unit: psu) in August (left column) and September (right column) 2016 from Exp0 (top line), ExpV2 (middle line), and ExpV3 (bottom line). The black isolines indicate the 28, 30, 32, 34 and 35 psu isolines.

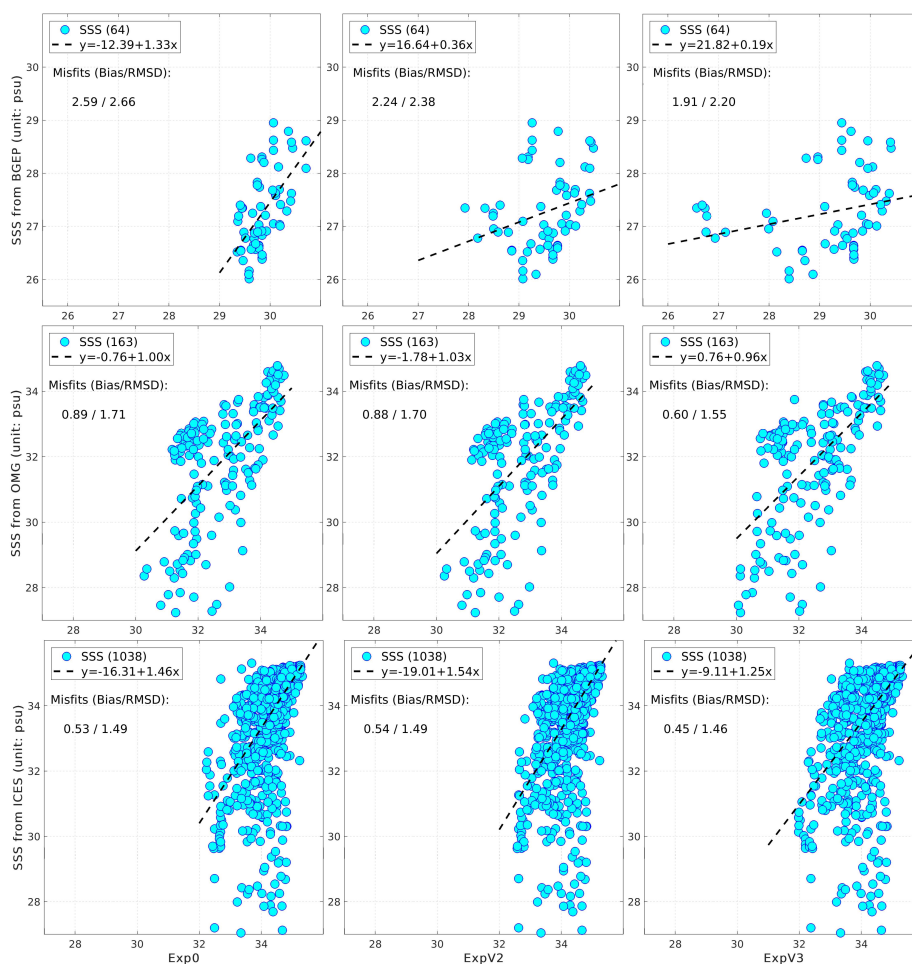


Fig. 4 Scatterplots of SSS in the TOPAZ assimilation runs against in-situ profiles (Upper: from BGEP in the Beaufort Sea; Middle: from OMG in both Greenland Seas; Bottom: from ICES in the Nordic Seas as indicated in Fig.1 and descriptions in 2.1). The statistics of SSS misfits are indicated in each panel with the bias and the RMSD respectively, the number of observations is given between parentheses, and the dark dashed line represents the linear regression.

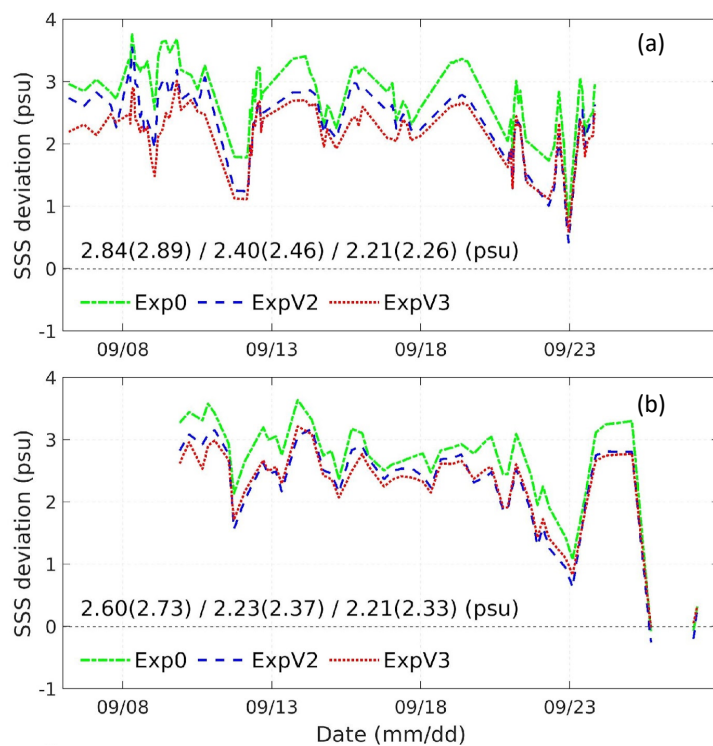


Fig. 5 Model-minus-observations SSS differences in the three assimilation runs against the SSS recorded in the Beaufort Sea and the Chukchi Sea along the SKQ cruise in 2016: a) from CTD profiles; b) from surface water samples underway in the same cruise. The biases are indicated in the same order and the corresponding RMSD between parentheses.

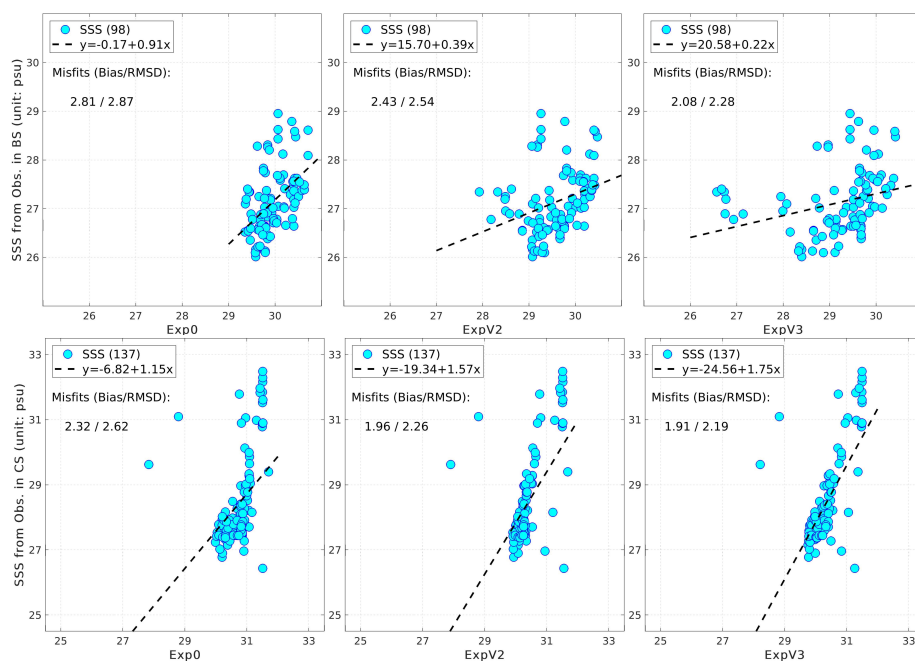


Fig. 6 Scatterplots of SSS (unit: psu) in the three assimilation runs of Exp0, ExpV2 and ExpV3 against the observations from the CTD profiles collected by different cruises in 2016. **Upper:** in the Beaufort Sea; **Bottom:** in the Chukchi Sea as shown in Fig.1.

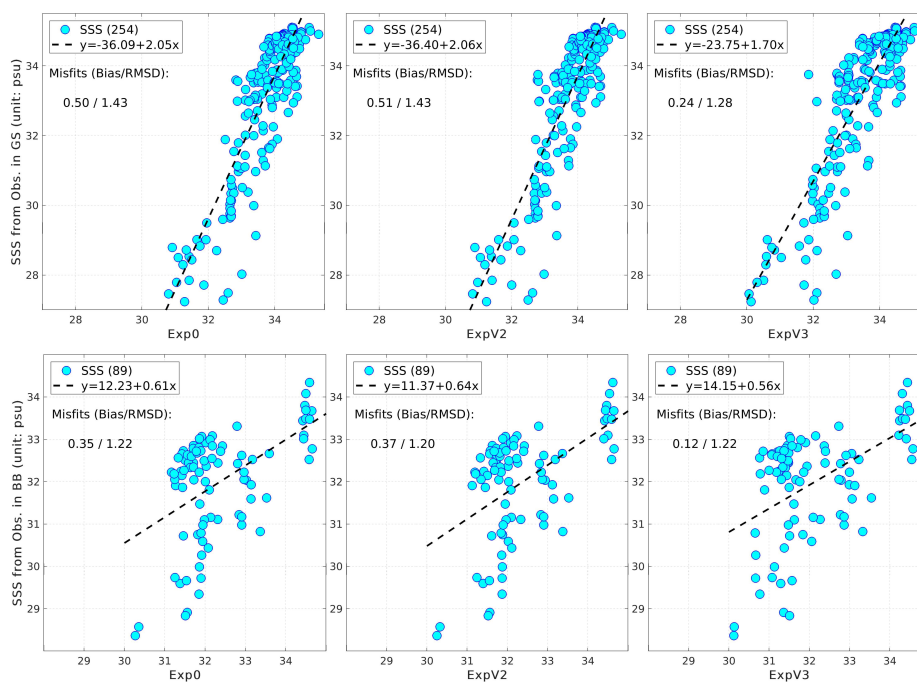


Fig. 7 Scatterplots of SSS (unit: psu) in the three assimilation runs of Exp0, ExpV2 and ExpV3 against the collected observations with the CTD profiles from OMG and ICES in 2016. **Upper:** in the Greenland East Sea; **Bottom:** in Baffin Bay as shown in Fig. 1.

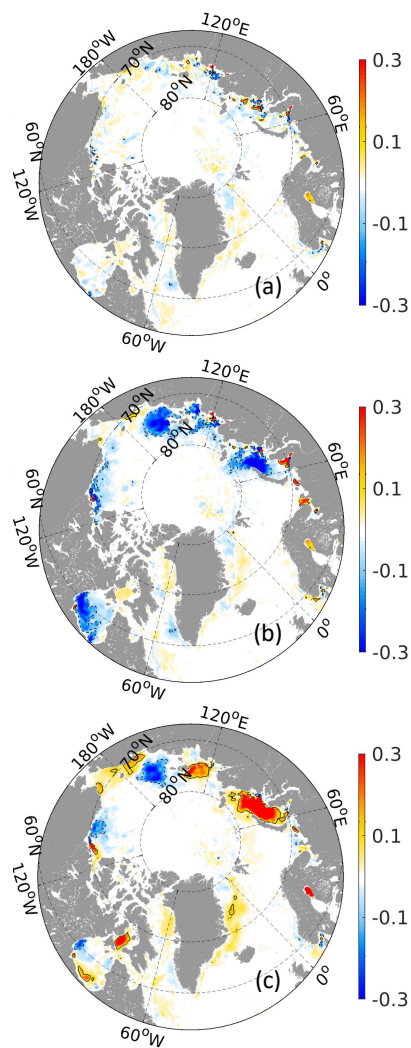


Fig 8. Averaged increment of SSS in Exp0 (a), ExpV2 (b) and ExpV3 (c). The obvious changes of SSS (± 0.1 psu) are highlighted by isolines.

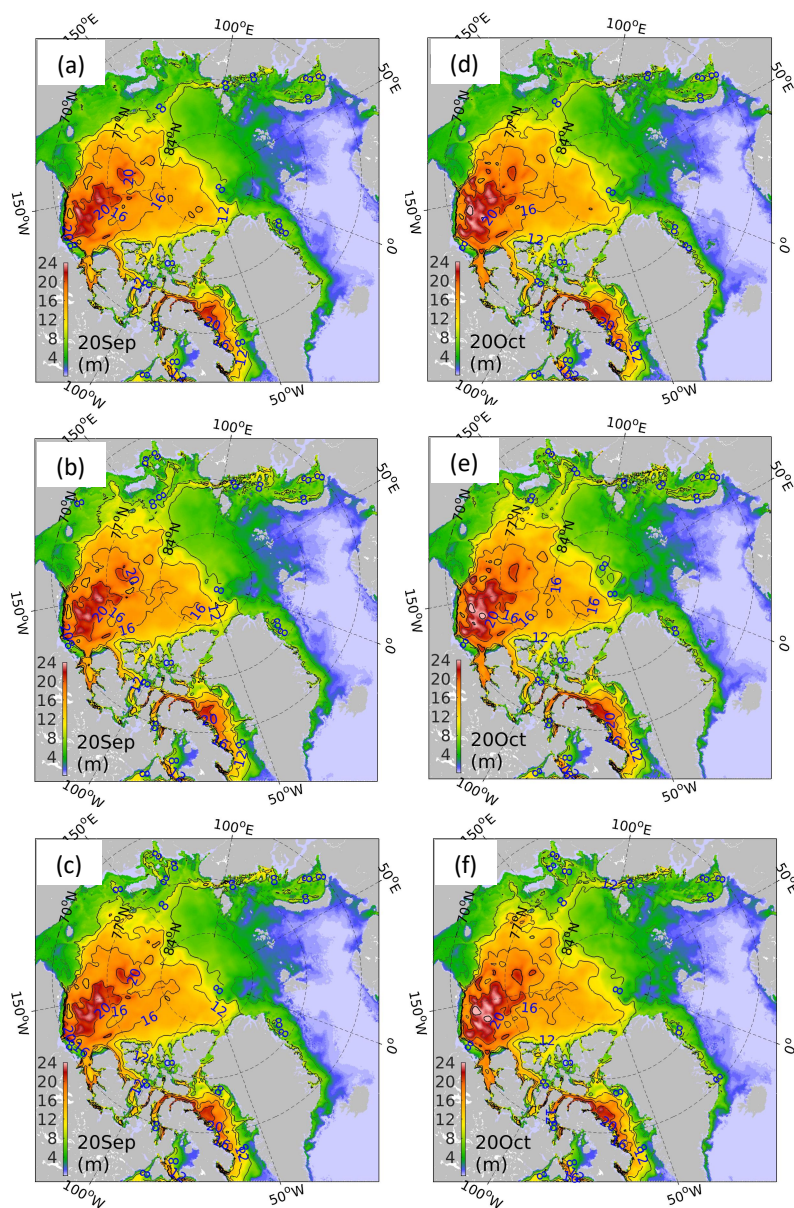


Fig 9. Daily freshwater content depths (unit: m) on 20th September and 20th October 2016 in Arctic Ocean from the three assimilation runs: Exp0 (a; d), ExpV2 (b; e), and ExpV3 (c; f). The interval of isolines is 4 meters.

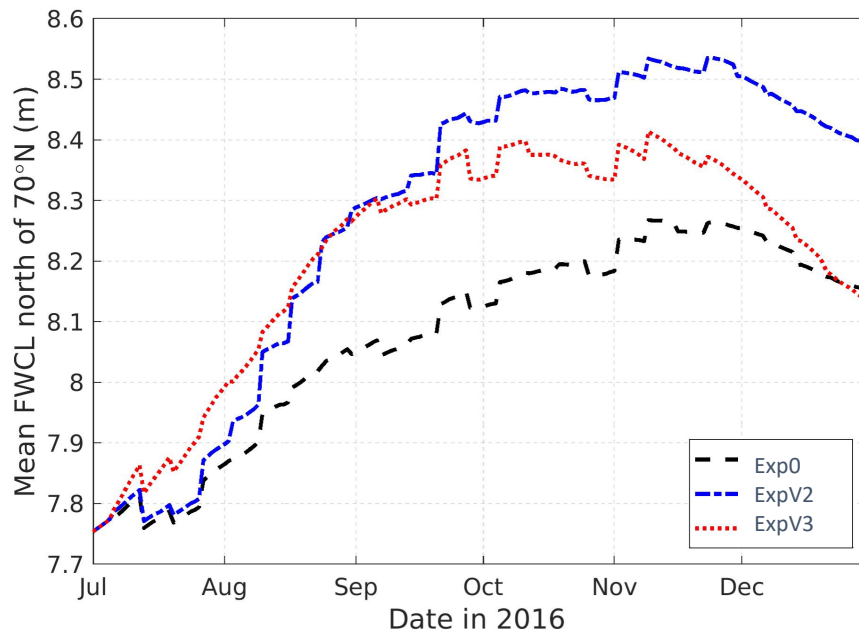


Fig 10. Mean freshwater content depths (unit: m) in the central Arctic (>70°N) during the period from July to December 2016 for Exp0 (dark dashed), ExpV2 (blue dashed), and ExpV3 (red dotted).